

# To Learn or Not to Learn: Visual Localization from Essential Matrices

Qunjie Zhou<sup>1</sup>    Torsten Sattler<sup>2</sup>    Marc Pollefeys<sup>3,4</sup>    Laura Leal-Taixé<sup>1</sup>  
<sup>1</sup>TU Munich    <sup>2</sup>Chalmers University of Technology    <sup>3</sup>ETH Zürich    <sup>4</sup>Microsoft

## Abstract

*Visual localization is the problem of estimating a camera within a scene and a key component in computer vision applications such as self-driving cars and Mixed Reality. State-of-the-art approaches for accurate visual localization use scene-specific representations, resulting in the overhead of constructing these models when applying the techniques to new scenes. Recently, deep learning-based approaches based on relative pose estimation have been proposed, carrying the promise of easily adapting to new scenes. However, it has been shown such approaches are currently significantly less accurate than state-of-the-art approaches. In this paper, we are interested in analyzing this behavior. To this end, we propose a novel framework for visual localization from relative poses. Using a classical feature-based approach within this framework, we show state-of-the-art performance. Replacing the classical approach with learned alternatives at various levels, we then identify the reasons for why deep learned approaches do not perform well. Based on our analysis, we make recommendations for future work.*

## 1. Introduction

Given a query image, the goal of visual localization problem is to estimate its camera pose, *i.e.*, the position and orientation from which the query photo was taken, in a given scene. Visual localization is a fundamental problem in Computer Vision, encountered for example in Structure-from-Motion (SfM) [64, 79] and Simultaneous Localization and Mapping (SLAM) [21, 47], and has applications in robotics, *e.g.*, autonomous vehicles [40, 42], as well as Augmented Reality [3, 13].

Current approaches to visual localization that achieve state-of-the-art pose accuracy are based on 3D information [5, 7, 14, 45, 60, 65, 70, 71]: They first establish 2D-3D matches between 2D pixel positions in a query image and 3D points in the scene. The resulting correspondences are then used to estimate the camera pose for the query image using a  $n$ -point-pose solver, *e.g.*, a 3-point solver [34] for calibrated cameras, in a RANSAC [22] loop.

The 3D scene geometry used in the matching stage can be represented either explicitly or implicitly. In the former case, each 3D point is associated with local image descriptors such as SIFT [41], *e.g.*, as part of reconstructing the scene via SfM, and 2D-3D matches are established via descriptor matching. In the latter case, the 3D scene geometry is stored implicitly in the weights of convolutional neural networks (CNNs) [5, 7] or through a random forest [6, 14, 24, 45, 67, 76]. The drawback of such methods is that they are based on scene-specific information, *i.e.*, a new 3D model needs to be build or a new CNN trained for each new scene. In addition, the representations need to be updated every time the scene changes, which can be computationally expensive [62].

A more flexible scene representation models a scene through a set of database images with associated camera poses [62]. This is the minimal amount of information needed to infer the 3D scene geometry and at the same time as easy to update as simply adding more posed images [62]. A simple way to use this representation for localization is to approximate the pose of a query image by the pose of the most similar database image [1, 72], identified through image retrieval [51, 68], or a combination of the poses of the most similar images [73]. More accurate pose estimates can be obtained by triangulating the pose of the query image from relative poses to retrieved images [83], by using depth maps if available for absolute pose estimation [70], or by performing a local SfM reconstruction [62]. Multiple methods based on deep learning and regression have been proposed for estimating the pose of the query relative to the database images [4, 35, 44, 75, 84] rather than to compute it explicitly from feature matches [83]. However, it was recently shown that such approaches do not consistently perform better than a simple retrieval approach that only approximates the query pose [63].

Visual localization approaches based on relative poses have desirable properties, namely simplicity and flexibility of the scene representation and easy adaption to new scenes, compared to 3D-based approaches. In addition, leveraging the power of modern machine learning techniques for relative pose estimation seems a natural thing to do. This leads to the question why learning-based approaches do not per-

form well in this setting.

To analyze the performance of relative pose regression approaches, we propose a generic framework for visual localization based on relative poses. More precisely, we describe a pipeline based on essential matrices (as we show that regressing essential matrices rather than relative poses has advantages) that uses a novel RANSAC approach to easily handle the resulting ambiguities. Our framework is agnostic to the way the essential matrices are estimated. We thus use it to analyze the impact of employing machine learning in various ways when computing the essential matrices: (a) Following classical approach based on matching SIFT features [41] and estimating the essential matrix via the 5-point solver [49] inside a RANSAC loop. (b) Directly regressing an essential matrix using a novel CNN-based approach. (c) A hybrid approach that uses learned feature matching in combination with 5-point-based essential matrix estimation. Through detailed experiments, we show three observations: 1) Our SIFT-based approach (a), despite its simplicity, is competitive with respect to significantly more complex state-of-the-art approaches [7, 60, 70], thus validating our framework. 2) Our regression-based approach (b), although outperforming previous work, is still significantly worse than the SIFT-based variant. In particular, it does not generalize to unseen scenes due to the inability of its regression layers to learn the general concepts underlying relative pose estimation. 3) While the regression layer is mainly responsible for the inaccurate pose estimates of relative pose regression-based methods, it is not the only part that needs improvements. Rather, using features learned by such methods in our hybrid approach (c) also leads to less accurate results compared to (a).

Besides proposing a novel localization framework based on relative poses, this paper thus also contributes important insights into future work towards truly generalizable learning-based visual localization.

## 2. Related work

**Feature-based localization.** Feature-based approaches to visual localization can be classified into *direct* [12, 15, 37, 38, 42, 60, 69, 82] and *indirect* [2, 11, 28, 59, 72, 74, 80, 81, 83] approaches. The former follow the strategy outlined above and obtain 2D-3D matches by directly comparing feature descriptors extracted from a query image with 3D points in the SfM model. While producing accurate camera pose estimates, the drawback of these approaches is that they need to keep all 3D point descriptors in memory, limiting their scalability to larger scenes. This limitation can partially be overcome by compressing the scene model, by removing 3D points [10, 12, 38] or by compressing point descriptors [10, 42, 59]. Yet, model compression typically reduces the percentage of images that can be localized [12, 42].

Rather than directly matching descriptors, *indirect* approaches first perform an image retrieval step [29, 51, 68] against the database images used to build the SfM model to determine which parts of a scene are visible in a query image. The pose of the query image can then be approximated by the pose of the most similar database image [62, 72] or by interpolating between the poses of multiple retrieved images [80]. A more accurate pose estimate can be obtained by restricting descriptor matching to the points visible in the top-retrieved images [28, 59, 70], which can be done memory efficient by loading the relevant parts from disc. The advantage of indirect methods is that the retrieval step can be done very efficiently (both in terms of memory and run-time) using compact image-level descriptors [1, 52, 72]. At the same time, it is not strictly necessary to store a 3D scene representation to obtain accurate pose estimates: Given the known poses of the database images, it is possible to compute the query pose via constructing and geo-registering a local SfM model from scratch [62] or by triangulating the position of the query image from relative poses w.r.t. the database images [83].

**Machine learning in visual localization.** Retrieval methods [1, 11, 23] have benefitted greatly from deep learning architectures. Several works have been proposed to directly learn the 2D-3D matching function [5, 7, 14, 20, 24, 67, 76]. While traditionally a dense 3D scene model is required for training, a recent work has shown that similar accuracy can be achieved without the need of a 3D model during training [7]. The main drawback of these approaches, besides having problems scaling to larger scenes [7, 66], is that the learned models are scene-dependent as they regress 3D coordinates. Recent work has shown the ability to adapt a model trained on one scene to new scenes on-the-fly [14]. Yet, [14] considers the problem of re-localization against a trajectory while we consider the problem of localization from a single image.

**Learning absolute pose estimation.** Recent works have proposed to learn the complete localization pipeline, by either modeling localization as a classification problem [78] or learning to directly regress the absolute pose of a query image [30–32, 43, 48, 77]. These methods typically only require images and their corresponding camera poses as training data and minimize a loss on the predicted camera poses [31, 32]. At the same time, it has been shown that using 2D-3D matches as part of the loss function can lead to more accurate results [31]. Similar to the approaches described above, the learned representations are scene-dependent and do not generalize.

**Learning relative pose estimation.** The authors of DeMoN [75] propose a CNN that jointly predicts a depth map for one image and the relative pose w.r.t. to a second image. They require depth maps for training, whereas our ap-

proach does not. An unsupervised variant of DeMoN that is trained purely on a stream of images by using image synthesis as a supervisory loss function is presented in [84]. The method is tested in an autonomous driving scenario that exhibits planar motion and it is unclear how well this approach would work in the 6DOF scenario with larger baselines considered in this paper.

An image representation suitable for camera pose prediction based on frustum overlap is proposed in [4]. Their network is jointly trained for the tasks of image retrieval and relative camera pose regression. Different from other pose learning methods, they parametrize a relative camera pose as a  $\mathbb{SE}(3)$  transformation and minimize the logarithm of distance between the predicted and the ground truth transformation. However, their method directly learns the scale of the relative translation in the transformation matrix, so it is unclear whether a single network could work for both small-scale indoor as well as large-scale outdoor environments. Most similar in spirit to our approach, [35] first identifies potentially relevant database images based on the similarity of the extracted feature descriptors. A network is then trained to estimate the relative poses between the query image and the retrieved database photos, followed by triangulation to estimate the query’s absolute camera pose inside a RANSAC loop. As we detail in our work, regressing essential matrices is a better choice and we show how to handle pose ambiguity directly inside the RANSAC loop. We analyze which parts of the localization pipeline fail when replaced by a data-driven approach, showing that learning the whole pipeline as in [35] is by far not the most accurate solution.

### 3. Essential Matrix Based Localization

In this section, we propose a scalable pipeline to estimate the absolute pose of a query image w.r.t. to a scene represented by a database of images with associated camera poses. Our pipeline, shown in Fig. 1, consists of three stages: In the first stage, we use image retrieval to identify a set of images that potentially depict the same part of the scene as the query image (*c.f.* Sec. 3.1). For each retrieved image, we compute the essential matrix that encodes its relative pose with respect to the query image (*c.f.* Sec. 3.2). Finally, using the known absolute poses of the retrieved images, we are able to triangulate the position of the query image and estimate its orientation (*c.f.* Sec. 3.3). Similar in spirit to our work, Zhou *et al.* [83] retrieve images and then triangulate the pose of a query from two database images using a fundamental matrix or homography, while we formalize it inside our RANSAC.

**Why essential matrices?** Since we are ultimately interested in extracting relative poses, one might wonder why not training a CNN to directly predict relative poses instead

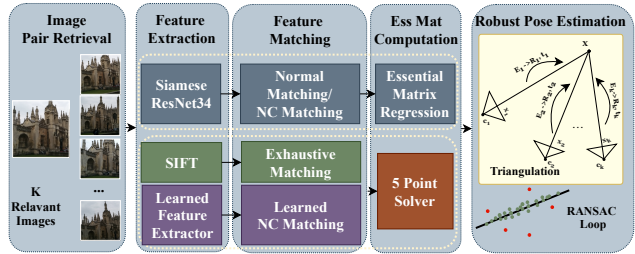


Figure 1. Our localization pipeline. Given a query image, the pipeline first retrieves top-k similar training images using DenseVLAD descriptors, composing k input pairs. In the next stage, we propose 3 approaches(Sec. 4) to estimate K essential matrices from the pairs, which are fed into our RANSAC loop for relative pose extraction as well as the absolute pose computation.

of essential matrices. Several works [4, 35, 58] propose a model for relative pose prediction, with the main disadvantage of needing a scene-dependent hyperparameter to weight the translation and orientation losses (*c.f.* Sec. 4.2).

We propose to estimate essential matrices as an intermediate step. This is motivated by the way classical methods estimate essential matrices: First obtain 2D-2D feature matches and then recover the relative pose up to an arbitrary scaling factor. In the supplementary material, we show that directly regressing essential matrix automatically resolves the scene-dependent weighting issue from relative pose regression and also leads to more accurate results. While directly decomposing the essential matrix into relative poses results in ambiguities, we propose in Sec. 3.3 how to handle it inside a RANSAC loop.

In the following sections, we do not focus on the method used for essential matrix estimation, but rather presenting a complete pipeline for localization based on essential matrices, without the need for a 3D model. We will discuss multiple approaches to essential matrix estimation in Sec. 4.

**Notation.** The absolute camera pose ( $R_{\mathcal{I}}, \mathbf{t}_{\mathcal{I}}$ ) of an image  $\mathcal{I}$  is defined by a rotation matrix  $R_{\mathcal{I}}$  and a translation  $\mathbf{t}_{\mathcal{I}}$  such that  $R_{\mathcal{I}}\mathbf{x} + \mathbf{t}_{\mathcal{I}}$  transforms a 3D point  $\mathbf{x}$  from a global coordinate system into the local camera coordinate system of  $\mathcal{I}$ . Accordingly, the camera center  $\mathbf{c}_{\mathcal{I}}$  of  $\mathcal{I}$  in global coordinates is given by  $\mathbf{c}_{\mathcal{I}} = -R_{\mathcal{I}}^T \mathbf{t}_{\mathcal{I}}$ . Notice that in practice, we are representing the rotation  $R_{\mathcal{I}}$  by a quaternion  $\mathbf{q}_{\mathcal{I}}$ . As such, we will interchangeably use either a rotation matrix  $R$  or a quaternion  $\mathbf{q}$  to denote a (relative or absolute) rotation.

#### 3.1. Retrieving Relevant Database Images

We perform image retrieval run-time and memory efficiently by representing each database image by DenseVLAD descriptors [72]. DenseVLAD has been shown to perform retrieval accurately [62] and work under challenging conditions [61]. Compared to other learned pipelines for image retrieval [52, 53], DenseVLAD shows better generalization to unseen scenes, which fits well to our pipeline.

**Pair selection.** Simply picking top-k nearest neighbors to a query image is not sufficient to obtain good performance in our experiments, since retrieved database images are often too close to each other to guarantee robust triangulation. To ensure a larger baseline distance between the retrieved images and the query image while still keeping enough visual overlapping, we add minimal/maximal distance thresholds between the previous and current retrieved images. Each of the retrieved training images and the query image composes an image pair, from which we estimate an essential matrix (c.f. Sec. 4.2). Note, that not all pairs generated by retrieval are necessarily valid, *i.e.*, the two images in a pair might just have a similar overall appearance but do not actually show the same part of the scene. We handle such outliers via RANSAC [22] as detailed in Sec. 3.3.

### 3.2. Pairwise Relative Pose Estimation

For each image pair, we first compute the essential matrix  $E$  that encodes the relative pose between the query and database image. Next, we use SVD to extract the four relative poses  $(R, \mathbf{t}), (R, -\mathbf{t}), (R', \mathbf{t}), (R', -\mathbf{t})$  corresponding to  $E$  [25], where  $R$  and  $R'$  are related by a  $180^\circ$  rotation around the baseline [25]. Traditionally, the correct pose among the four is identified through a cheirality test: Given the feature matches used to estimate  $E$ , the four poses are used to triangulate 3D points. Next, the pose is selected for which all 3D points are in front of both cameras. However, there are cases for which we do not have explicit image correspondences, *e.g.*, for our regression models in Sec. 4.2. Interestingly, once the essential matrix is predicted, is it only necessary to disambiguate the rotation part. As described in Sec. 3.3, we use the estimated translation directions to triangulate the absolute pose of a query image from two or more image pairs. At the same time, the position of a point triangulated from multiple directions  $\mathbf{t}_1, \dots, \mathbf{t}_n$  does not change when flipping the signs of any direction  $\mathbf{t}_i$ . Thus, the absolute position of the query image can be uniquely determined by  $n$  images pairs, with  $n \geq 2$  assuming not all images are colinear.

Let  $R_i$  and  $R'_i$  be the relative rotations from the  $i$ -th retrieved database image - query image pair  $(\mathcal{I}_i, \mathcal{I}_q)$ . Here, both rotations transform from the local coordinate system of  $\mathcal{I}_i$  into the local coordinate system of  $\mathcal{I}_q$ . Thus, the rotation transforming from the global coordinate system to the local system of the query image is either  $R_i R_{\mathcal{I}_i}$  or  $R'_i R_{\mathcal{I}_i}$ .

Consider a second image pair  $(\mathcal{I}_j, \mathcal{I}_q)$  under the condition that the camera centers of  $\mathbf{c}_{\mathcal{I}_i}$ ,  $\mathbf{c}_{\mathcal{I}_j}$ , and  $\mathbf{c}_{\mathcal{I}_q}$  are not collinear. Given exact essential matrices  $E_i$  and  $E_j$ , two of the four absolute rotations  $R_i R_{\mathcal{I}_i}$ ,  $R'_i R_{\mathcal{I}_i}$ ,  $R_j R_{\mathcal{I}_j}$ ,  $R'_j R_{\mathcal{I}_j}$  have to be identical. In practice, the rotations will not be identical. However, the angle between the two rotations in one of the four possible pairs  $(R_i R_{\mathcal{I}_i}, R_j R_{\mathcal{I}_j}), (R_i R_{\mathcal{I}_i}, R'_j R_{\mathcal{I}_j}), (R'_i R_{\mathcal{I}_i}, R_j R_{\mathcal{I}_j}), (R'_i R_{\mathcal{I}_i}, R'_j R_{\mathcal{I}_j})$  will be small while the an-

gles of all other pairs will be large since  $R_i$  and  $R'_i$  (as well as  $R_j$  and  $R'_j$ ) are related by a  $180^\circ$  rotation. Therefore, the minimal angle among the four angles identifies the two consistent relative rotations for the two pairs as well as provides two absolute rotations hypotheses. The final absolute rotation hypothesis is the average of the two hypotheses. Notice that in the case where all three camera centers are collinear, there will be two pairs of consistent rotations.

### 3.3. Absolute Pose Estimation via RANSAC

Consider a pair  $((\mathcal{I}_i, \mathcal{I}_q), (\mathcal{I}_j, \mathcal{I}_q))$  of image pairs. Let  $R_q$  be the absolute rotation of the query image estimated from the two image pairs as described in the previous section. Furthermore, let  $R_i$  and  $R_j$  be the relative rotations consistent with  $R_q$ . Using the two relative translation directions  $\mathbf{t}_i$  and  $\mathbf{t}_j$ , we can determine the position of the query image via triangulation from the two rays  $\mathbf{c}_{\mathcal{I}_i} + \lambda_i R_{\mathcal{I}_i}^T R_i \mathbf{t}_i$  and  $\mathbf{c}_{\mathcal{I}_j} + \lambda_j R_{\mathcal{I}_j}^T R_j \mathbf{t}_j$  [25], where  $\lambda_i, \lambda_j \in \mathbb{R}$  are scalar factors defining points along the two rays. Notice that the result of triangulation is only defined if the three camera centers are not collinear. In practice, we use more than two database images to compute the final pose, hence this will only become a problem in certain scenarios where all images are taken on a line, *e.g.*, self-driving cars where the car is driving down a road.

As shown above, a hypothesis for the absolute pose of a query image can be estimated from two pairs. To be robust to outlier pairs, we use RANSAC [22]: In each iteration, we sample two pairs  $(\mathcal{I}_i, \mathcal{I}_q), (\mathcal{I}_j, \mathcal{I}_q)$  and use them to estimate the absolute pose hypothesis  $(R_{\mathcal{I}_q}, \mathbf{t}_{\mathcal{I}_q})$  of the query image. Next, we determine which image pairs are inliers to that pose hypothesis. For a pair  $(\mathcal{I}_k, \mathcal{I}_q)$  defining four relative poses between  $\mathcal{I}_k$  and  $\mathcal{I}_q$ , we first determine the relative rotation  $R_k$  that minimizes the angle between the absolute rotations  $R_{\mathcal{I}_q}$  and  $R_k R_{\mathcal{I}_k}$  (following the same reasoning as above). We then use  $R_k$  to measure how consistent the predicted relative pose is with the absolute pose hypothesis predicted by the image pair. The relative translation from  $\mathcal{I}_q$  to  $\mathcal{I}_k$  predicted by the pose  $(R_{\mathcal{I}_q}, \mathbf{t}_{\mathcal{I}_q})$  is given as  $\mathbf{t}_{\text{pred}} = R_{\mathcal{I}_k} (\mathbf{c}_{\mathcal{I}_q} - \mathbf{c}_{\mathcal{I}_k})$ .

We thus measure the consistency with the predicted relative translation  $\mathbf{t}_k$  via the angle  $\alpha = \cos^{-1}(\mathbf{t}_k^T \mathbf{t}_{\text{pred}} / (||\mathbf{t}_k||_2 ||\mathbf{t}_{\text{pred}}||_2))$ . If the angle between the two predicted translation directions is below a given threshold  $\alpha_{\text{max}}$ , we consider the pair  $(\mathcal{I}_k, \mathcal{I}_q)$  as an inlier.

We use local optimization [36] inside RANSAC to better account for noisy relative pose predictions. RANSAC finally returns the pose with the largest number of inliers.

## 4. Essential Matrix Estimation

Several methods exist in the computer vision literature that perform accurate visual localization with classical methods, showing good generalization, but still lacking

scalability and memory efficiency. While Deep Learning has made huge advances in other vision tasks such as image classification, in visual localization end-to-end trained methods are still far behind classic methods in terms of accuracy [63]. We are highly interested in understanding how to better leverage the power of data-driven methods to build a robust, scalable, flexible and generalizable localization pipeline. To this end, we propose different approaches for essential matrix estimation, ranging from purely hand-crafted models to purely data-driven ones. All methods will be tested inside the localization pipeline described in Sec. 3.

#### 4.1. Feature-based: SIFT + 5-Point Solver

We first propose to follow the classical feature-based method that extracts local features, *i.e.*, SIFT in this work, searches for feature matches between the query and a retrieved database image, and finally estimates the essential matrix via the 5-point solver inside RANSAC. To get essential matrix directly from correspondences, we assume we know the camera intrinsics. This approach serves as a baseline for standard accurate methods within our localization pipeline (*c.f.* Sec. 3). Note, that within our pipeline, we do not need an explicit dense 3D model of the scene to perform localization.

#### 4.2. Learning-based: Direct Regression via EssNet

A benefit of deep learning is the potential of a simple end-to-end trainable model, typically a neural network consisting of feature extraction layers and regression layers.

Unlike [9, 16, 30–32, 48, 77] which directly regress absolute poses and are shown to have limitations in generalization by definition [63], we are working with image pairs and want to implicitly estimate relative poses. More related to our work, [4, 35, 44] propose to directly regress the relative poses with siamese neural networks. Rather than working with relative poses, we propose to regress essential matrices, which has several advantages as discussed below.

**Issues with relative pose regression.** [35, 44] parametrize the pose with a rotation quaternion and a translation vector and use the following weighted loss function:

$$\mathcal{L}_w(y^*, y) = \|\mathbf{t} - \mathbf{t}^*\|_2 + \beta \|\mathbf{q} - \mathbf{q}^*\|_2, \quad (1)$$

where  $y^* = (\mathbf{q}^*, \mathbf{t}^*)$  is the relative pose label,  $y = (\mathbf{q}, \mathbf{t})$  is the relative pose prediction,  $\mathbf{q}$  is the relative rotation encoded in a 4D quaternion, and  $\mathbf{t}$  is the 3D translation. Commonly, the scale of  $\mathbf{t}$  is kept during training and the predicted translation is normalized to only preserve a direction [35, 44]. Notice, the  $\beta$  in  $\mathcal{L}_w$  is a hyperparameter to balance the learning between translation and rotation, which is scene-dependent (*e.g.*, its values differ significantly for indoor and outdoor scenes [32]). [44] performs grid search to find the optimal  $\beta$ , following other absolute pose methods [30, 32, 77]. In [35], authors find that setting  $\beta = 1.0$

works well for indoor scenes. The authors of [31] propose to learn the weighting parameter  $\beta$  from training data.

Rather than keeping working around the hyperparameter  $\beta$ , we propose to directly eliminate the weighting by regressing essential matrices. It is verified by our experiments (*c.f.* supplementary material) that this works as a more general solution, since it allows us to train a single model that works under various types of scenes.

**Proposed network architecture.** Siamese neural networks are a natural choice for relative pose estimation between two images, as they have two identical branches with shared weights to extract image features. As in [9, 35], we use ResNet34 [27] (until the last average pooling layer) as our architectural backbone. While [35, 44] directly regress relative poses from the concatenated feature maps using with the weighted loss function defined in Eq. 1, we first involve a *feature matching* step that resembles the process in classic feature-based localization methods [37, 60, 69, 82] after the feature extraction. We analyze two options for the matching step: 1) A simple fixed matching layer [55], essentially a matrix dot product between feature maps coming from the two images. 2) A learnable Neighborhood Consensus (NC) matching layer [56], which enforces neighbourhood consensus and mutual consensus constraints based on the normal matching layer [55] using 4D convolutions. Both matching versions combine the two feature maps into a single feature tensor that can be seen as a pairwise matching score map at feature map resolution. The score map is then fed to the regression layers which predict the essential matrix. These regression layers consist of two blocks of convolutional layers followed by batch normalization with ReLU, and finally a fully connected layer to regress a 9D vector which approximates the essential matrix.

**Projection layer.** To further enforce the internal constraints of an essential matrix, *i.e.*, having two equal singular values and the third one being zero, we use a projection layer. Following the common practice in any classic feature-based localization pipeline, it first performs SVD on the approximated essential matrix, then replaces the first two singular values with their mean value and finally sets the smallest singular value to 0. We use standard functionality provided by PyTorch [50] for SVD backpropagation, the same as [54] did.

We name the proposed models as **EssNet** (with simple matching layer) and **NC-EssNet** (with NC matching layer). We perform an ablation study (*c.f.* supplementary material) to validate our architectural design choice of EssNet. We show that matching layer is superior to simple concatenation operation to combine feature maps for essential matrix regression. Secondly, projection layer which brings an essential matrix approximation into a true one, also improves performance.

**Loss function.** For training, we use the loss function  $\mathcal{L}_{ess}$ , defined as the Euclidean distance between the predicted essential matrix  $E$  and the ground truth  $E^*$ :

$$\mathcal{L}_{ess}(E^*, E) = \|e - e^*\|_2. \quad (2)$$

Here, we represent each essential matrix  $E \in \mathbb{R}^{3 \times 3}$  as a 9D vector  $e \in \mathbb{R}^9$  obtained by stacking its elements. Given a relative camera pose label  $(R^*, t^*)$ , the ground truth essential matrix is  $E^* = [t^*]_{\times} R^*$ , where  $[t^*]_{\times}$  is the skew-symmetric matrix of the normalized translation label  $t^*$ , i.e.,  $\|t^*\| = 1$ . We assume that the intrinsic calibration for all images is known, therefore, we resize and crop all training and test images to have the same intrinsic calibration.

### 4.3. Hybrid: Learnable Matching + 5-Point Solver

Finally, we propose a hybrid of feature-based and learning-based methods, where feature extraction and feature matching are learned via neural networks, and then the 5-point algorithm inside a RANSAC loop is used to compute the essential matrix from the learned matches. In terms of architecture, we use the same matching layers as in NC-EssNet, i.e., NC-EssNet without the regression layers, leading to a matching network similar to the NC-Net model proposed in [56] (except for the feature extraction network, which is ResNet101 in their case).

With the proposed localization pipeline, we can now evaluate the quality of different essential matrix estimation methods in terms of localization performance.

## 5. Experiments

In the following, we evaluate our novel localization approach based on essential matrix estimation. In particular, we are interested in using our approach to analyze why methods based on relative pose regression do not generalize as theoretically expected. To this end, we first demonstrate that our approach, based on handcrafted features and RANSAC-based essential matrix estimation, achieves state-of-the-art performance (c.f. Sec. 5.1). We then use learned essential matrix estimation approaches inside our framework to analyze their weaknesses (c.f. Sec. 5.2). Finally, Sec. 5.3 discusses our results and draws conclusions for future work.

**Datasets and evaluation protocol.** We follow common practice and use the Cambridge Landmarks [32] and 7 Scenes [67] datasets for evaluation. For both datasets and all methods, we report the median absolute position error in meters and the median absolute rotation error in degrees.

**Implementation details.** We split 1/6 of the training set images as validation images to control the training process. To generate the training pairs required by EssNet and NC-

Method/Scenes	Indoor(t1/t2)	Outdoor(t1/t2)
(NC-)EssNet	-/5	-/5
SIFT+5Pt	0.5/15	0.5/5
Feat.*+NCM+5Pt	5.5/20	4.0/15

Table 1. Ransac thresholds used in our experiments. Feat.\* means any feature extractor.

EssNet, we use the CNN (resnet101-gem) proposed in [53] to retrieve training pairs (c.f. supplementary material).

EssNet and NC-EssNet are trained with exact the same settings for fair comparison. The ResNet34 layers are initialized with the model pre-trained on ImageNet [19]. The regression network layers are initialized with Kaiming initialization [26]. For each dataset, we train the model on training pairs from *all scenes* and evaluate per scene at test time. Note, that we use a single network to test on all Cambridge Landmarks sequences, while absolute pose methods [31, 32, 48, 77] train a separate network per sequence. All training images are first rescaled so that the shorter side has 480 pixels and then random cropped for training and center cropped for testing to  $448 \times 448$  pixels. All models are trained using AdamOptimizer [33] with learning rate  $1e^{-4}$  and weight decay  $1e^{-6}$  in a batch size of 16 for at most 200 epochs. We early stop training if overfitting is observed and use the model with best validation accuracy. The code is implemented using Pytorch [50] and executed on NVidia TITAN Xp GPUs.

During testing, we use DenseVLAD [72] to identify 5 most similar training images for each query image. The retrieved images have to satisfy the following condition designed to avoid retrieving close-by views and thus acute triangulation angles: Starting from the top-ranked image, we select the next image that has a distance within  $[a, b]$  meters to all previously selected images. For outdoor scenes  $a = 3, b = 50$  and for indoor scenes  $a = 0.05, b = 10$ . We show the choice of RANSAC thresholds  $t1$  in the 5-point algorithm [49] to distinguish inliers and outliers and  $t2$  in our RANSAC algorithm (c.f. Sec. 3.3) to remove outlier pairs for absolute pose estimation in Tab. 1. The thresholds were chosen through grid-search to maximize localization accuracy.

### 5.1. Comparison with State-of-the-Art

To validate our pipeline based on essential matrix estimation, we compare results obtained with our approach to state-of-the-art methods on the Cambridge Landmarks and 7 Scenes datasets. We focus on the results obtained when using SIFT features and the 5-point solver for estimating the essential matrices (c.f. Sec. 4.1). We use COLMAP [64] to extract and match features and the 5-point RANSAC implementation provided in OpenCV [8].

We compare our approach to methods for absolute pose regression (APR) [9, 30–32, 77], relative pose regression (RPR) [4, 35, 58], the two image retrieval (IR) baselines

based on DenseVLAD [72]<sup>1</sup> used in [63], and two state-of-the-art structure-based methods (3D) that explicitly estimate 2D-3D matches [7, 60]. For two RPR methods, we report results obtained when training on the 7 Scenes dataset (7S) and when training on an unrelated dataset (University (U) [35] and ScanNet (SN) [17]).

As can be seen in Tab. 2, our approach (SIFT+5Pt) consistently outperforms all IR and APR methods. It outperforms all RPR approaches except for on Stairs scene and AnchorNet [58], yet our position accuracy is better than it on all other scenes. AnchorNet explicitly encodes a set of anchor points, which correspond to a subset of all training images, in the network and estimates the pose of a test image with respect to these anchors. As such, it needs to be trained explicitly per scene. In contrast, our SIFT+5Pt approach does not require any training at all and can easily be adapted to new scenes.

Compared to structure-based methods (3D), our approach performs competitively when taking into account that both Active Search and DSAC++ need to build a scene-specific model. In contrast, our approach just operates on posed images without the need for using any 3D structure. Specifically, with the exception of the Stair sequence, SIFT+5Pt performs similar to Active Search. DSAC++ is more accurate at the cost of expensive training with training times in the order of days, while our approach is lightweight and does not require any training.

## 5.2. Analyzing Relative Pose Regression (RPR)

One motivation for our localization pipeline was to understand why RPR methods perform worse compared to structure-based methods. In the following experiment, we thus use (NC-)EssNet, the approach for relative pose regression proposed in Sec. 4.2, to estimate the relative poses.

**Comparison with state-of-the-art.** We evaluate two variants: EssNet uses a simple matching layer [55] to correlate CNN features, while NC-EssNet uses the more advanced correlation layer proposed in [56]

In general, we observe that using the NC layer improves performance over the standard matching layer. As can be seen in Tab. 2, EssNet and NC-EssNet perform similar or better than both Relative PN and RelocNet, which also do not need to build a scene-specific model. In addition, our approaches are either competitive or better than APR and RPR methods that train a scene-specific representation. This shows that EssNet and NC-EssNet are state-of-the-art RPR methods, therefore, the insights of the experiments in the next paragraphs would also apply to other RPR works.

**The failure to generalize.** The promise of approaches based on relative pose regression [4, 35] compared to ab-

solute pose regression, is generalization to new scenes: An absolute pose estimate is scene-specific as it depends on the coordinate system used. In contrast, a network that learns to regress a pose relative to another image could learn general principles that generalize to unseen scenes.

Tab. 3 analyzes the ability of EssNet and NC-EssNet to generalize from indoor to outdoor scenes and vice versa. As can be seen, there is a substantial gap in pose accuracy compared to training on the same scenes and especially compared to the classical variant (SIFT+5Pt) of our pipeline. This clearly indicates that EssNet and NC-EssNet fail to learn a general underlying principle. As similar observation can be made for Relative PN [35] and RelocNet [4] in Tab. 2 by comparing their performance when trained on 7 Scenes (7S) with their performance when trained on another indoor dataset (U or SN).

Looking at Tab. 3 and Tab. 2, the important question to ask is why RPR methods fail to generalize: Do the features extracted in their base networks fail to generalize, is there a lack of generalization in the layer that regresses the relative pose, or is it a combination of both? In order to better understand the behavior of EssNet and NC-EssNet, we consider the hybrid version of our pipeline introduced in Sec. 4.3.

The hybrid variant uses NC matching layer (NCM) trained on ivd dataset [56] to extract feature matches. To analyze the impact of the feature extraction on the generalization performance, we train our ResNet34 backbone in different ways and on multiple datasets: On ImageNet [57] for image classification (IC) task, which corresponds to the pretrained model, and for the essential matrix regression (EMR) task on the ScanNet(SN) (indoor), MegaDepth(MD) (outdoor), 7 Scenes(7S) (indoor), and Cambridge Landmarks(CL) (outdoor) datasets. As we did in Ablation study (*c.f.* supplementary material), we train EssNet with reduced resolution, *i.e.*  $224 \times 224$ , on large datasets, *i.e.*, MegaDepth and ScanNet, in order to make training computationally feasible. We denote these models with EssNet224. Note that for our hybrid, we perform inference with the original high resolution images across all datasets.

Tab. 4 evaluates the performance of the different training strategies on the localization accuracy of our hybrid approach. As can be seen, there is little variation in performance independently how the features are trained. This clearly shows that the features themselves generalize well and that the failure to generalize observed in Tab. 3 is caused by the regression layer.

## 5.3. Discussion

The previous experiments have shown that relative pose regression approaches fail to generalize to unseen scenes due to the inability of the regression layers to generalize. This suggests that future research should abandon regression layers in favor of layers that estimate fundamental / es-

<sup>1</sup>DenseVLAD + Inter. denotes interpolating between the top-ranked database images. See [63] for details.

		Cambridge Landmarks				7 Scenes						
		Kings	Old	Shop	St. Mary's	Chess	Fire	Heads	Office	Pumpkin	Kitchen	Stairs
IR	DenseVLAD [72]	2.80/5.72	4.01/7.13	1.11/7.61	2.31/8.00	0.21/12.5	0.33/13.8	0.15/14.9	0.28/11.2	0.31/11.3	0.30/12.3	0.25/15.8
	DenseVLAD + Inter. [63]	1.48/4.45	2.68/4.63	0.90/4.32	1.62/6.06	0.18/10.0	0.33/12.4	0.14/14.3	0.25/10.1	0.26/9.42	0.27/11.1	0.24/14.7
3D	*Active Search [60]	0.42/0.55	0.44/1.01	0.12/0.40	0.19/0.54	0.04/1.96	0.03/1.53	0.02/1.45	0.09/3.61	0.08/3.10	0.07/3.37	<b>0.03/2.22</b>
	*DSAC++ [7]	<b>0.18/0.3</b>	<b>0.20/0.3</b>	<b>0.06/0.3</b>	<b>0.13/0.40</b>	<b>0.02/0.50</b>	<b>0.02/0.90</b>	<b>0.01/0.80</b>	<b>0.03/0.70</b>	<b>0.04/1.10</b>	<b>0.04/1.10</b>	0.09/2.60
APR	*PoseNet (PN) [32]	1.92/5.40	2.31/5.38	1.46/8.08	2.65/8.48	0.32/8.12	0.47/14.4	0.29/12.0	0.48/7.68	0.47/8.42	0.59/8.64	0.47/13.8
	*Learn. PN [31]	0.99/1.06	2.17/2.94	1.05/3.97	1.49/3.43	0.14/4.50	0.27/11.8	0.18/12.1	0.20/5.77	0.25/4.82	0.24/5.52	0.37/10.6
	*Bay. PN [30]	1.74/4.06	2.57/5.14	1.25/7.54	2.11/8.38	0.37/7.24	0.43/13.7	0.31/12.0	0.48/8.04	0.61/7.08	0.58/7.54	0.48/13.1
	*Geo. PN [31]	0.88/1.04	3.20/3.29	0.88/3.78	1.57/3.32	0.13/4.48	0.27/11.3	0.17/13.0	0.19/5.55	0.26/4.75	0.23/5.35	0.35/12.4
	*LSTM PN [77]	0.99/3.65	1.51/4.29	1.18/7.44	1.52/6.68	0.24/5.77	0.34/11.9	0.21/13.7	0.30/8.08	0.33/7.00	0.37/8.83	0.40/13.7
	*MapNet [9]	1.07/1.89	1.94/3.91	1.49/4.22	2.00/4.53	0.08/3.25	0.27/11.7	0.18/13.3	0.17/5.15	0.22/4.02	0.23/4.93	0.30/12.1
	*MapNet+PGO [9]					0.09/3.24	0.20/9.29	0.12/8.45	0.19/5.42	0.20/4.94	0.20/4.94	0.27/10.6
RPR	Relative PN [35] (U)					0.31/15.0	0.40/19.0	0.24/22.2	0.38/14.1	0.44/18.2	0.41/16.5	0.35/23.6
	Relative PN [35] (7S)					0.13/6.46	0.26/12.7	0.14/12.3	0.21/7.35	0.24/6.35	0.24/8.03	0.27/11.8
	RelocNet [4] (SN)					0.21/10.9	0.32/11.8	0.15/13.4	0.31/10.3	0.40/10.9	0.33/10.3	0.33/11.4
	RelocNet [4] (7S)					0.12/4.14	0.26/10.4	0.14/10.5	0.18/5.32	0.26/4.17	0.23/5.08	0.28/7.53
	*AnchorNet [58]	0.57/0.88	1.21/2.55	0.52/2.27	1.04/2.69	0.06/3.89	0.15/10.3	0.08/10.9	0.09/5.15	0.10/2.97	0.08/4.68	0.10/9.26
Ours	Sift+5Pt	0.48/1.13	0.88/1.91	0.17/0.99	0.35/1.58	0.04/2.42	0.05/2.85	0.04/3.86	0.06/2.66	0.08/3.81	0.07/3.12	0.22/11.08
	EssNet	0.76/1.89	1.39/2.78	0.84/4.3	1.32/4.66	0.13/5.14	0.27/10.13	0.15/9.90	0.21/6.89	0.22/6.13	0.23/6.87	0.32/11.18
	NC-EssNet	0.61/1.57	0.95/2.65	0.70/3.41	1.12/3.64	0.12/5.63	0.26/9.64	0.14/10.66	0.20/6.68	0.22/5.72	0.22/6.31	0.31/7.88
	NC-EssNet(7S)+NCM+5Pt	0.80/3.02	1.79/4.93	0.24/1.72	0.52/2.73	0.12/5.80	0.19/9.47	0.08/9.57	0.18/6.51	0.26/7.48	0.16/6.93	0.34/14.19
	Imagenet+NCM+5Pt	0.78/2.49	1.84/7.9	0.26/1.89	0.55/3.23	0.11/5.29	0.18/8.79	0.08/9.74	0.18/7.18	0.27/8.47	0.15/7.13	0.41/11.24
	EssNet224(SN)+NCM+5Pt	0.77/2.58	1.83/4.17	0.23/2.11	0.49/3.02	0.12/5.44	0.18/9.36	0.08/9.24	0.17/6.79	0.24/8.25	0.16/6.61	0.39/13.71

Table 2. Results on the Cambridge Landmarks [32] and 7 Scenes [67] datasets. We report the median position (in meters) / orientation (in degrees) errors. Methods marked with a \* build a scene-specific representation and need to be adapted / trained specifically for each scene.

Essential Matrix Estimation	Training Data	Testing Data	
		Cambridge	7Scenes
EssNet	Cambridge	1.08/3.41	0.57/80.06
NC-EssNet	Cambridge	0.85/2.82	0.48/32.97
EssNet	7Scenes	10.36/85.75	0.22/8.03
NC-EssNet	7Scenes	7.98/24.35	0.21/7.50
SIFT+5Pt	-	0.47/1.40	0.08/4.26

Table 3. Generalization study of regression models. We show average median position (in meters) / orientation (in degrees) errors.

Feature Matching	Train Task	Train Data	Cambridge	7Scenes
ImageNet+NCM	IC	ImageNet [57]	0.85/3.08	0.20/8.26
NC-EssNet+NCM	EMR	7S	0.84/3.10	0.19/8.56
NC-EssNet+NCM	EMR	CL	0.86/3.70	0.20/9.54
EssNet224+NCM	EMR	MD [39]	0.93/3.03	0.21/9.55
EssNet224+NCM	EMR	SN [17]	0.83/2.97	0.19/8.49
EssNet224+NCM	EMR	MD+7S+CL	0.86/3.20	0.22/10.30
SIFT+5Pt	-	-	0.47/1.41	0.08/4.27

Table 4. Evaluating the impact of trained features on localization performance when using different training strategies. We show average median position (in meters) / orientation (in degrees) errors.

essential matrices in trainable manner [18, 46, 54]. However, integrating such layers into a network that can be trained in an end-to-end manner does not seem straight-forward.

[18, 46, 54] perform relative pose estimation via iteratively re-weighted least-squares: The actual pose is estimated using a classical approach [25] while the weights are provided by a trainable network. Naturally, the pose accuracy that can be achieved will depend on how accurately the 2D measurements of the 2D-2D matches are localized in the images. In this regard, we make an interesting observation. As can be seen in Tab. 4, using trained features instead of SIFT features leads to significantly less accurate poses. This is due to the fact that the CNN features are less accu-

rately localized in the images compared to SIFT keypoints. This is evident from Tab. 1, which shows the best performing inlier threshold for RANSAC ( $t_1$ ) that we found for the two methods. This suggest that simply integrating a trainable pose estimation layer might not automatically lead to more accurate pose estimates with respect to SIFT. Rather, it might be necessary to develop more accurate feature networks, which might further complicate the integration of feature extraction, matching, and pose estimation into a single end-to-end network.

## 6. Conclusion

In this paper, we have proposed a novel framework for visual localization from essential matrices. Our approach is light-weight and flexible in the sense that it does not use information about the 3D scene structure model of the scene and can thus easily be applied to new scenes. Our results show that our framework can achieve state-of-the-art results. We have evaluated our framework using three different methods for computing essential matrices, ranging from purely hand-crafted to purely data-driven. By comparing their results, we have shown that the purely data-driven approach does not generalize well and have identified the reason for this failure as the relative pose regression layer. Furthermore, we have shown that the features and matches used by the data-driven approach themselves generalize quite well. However, directly using them for pose estimation yields less accurate results compared to the hand-crafted version of our pipeline. Based on our analysis, it is clear that more research is required before data-driven visual localization methods easily generalize to new scenes.

## Appendix

In this supplementary document, we first detail the data preprocessing and training pairs generation in Sec. 6 and Sec. 6 (*c.f.* main paper Sec.5). Next, we show a detailed ablation study for EssNet in Sec. 6 to validate our architectural choices (*c.f.* main paper Sec.3 & Sec.4.2). Finally, we show the effect of leveraging external datasets in EssNet performance in Sec. 6, which shows that EssNet is a general model to handle both indoor and outdoor scenes together (*c.f.* Sec.4.2).

### Dataset Preprocessing

For Cambridge Landmarks and 7Scenes, we did not do any preprocessing of the images. We use 1/6 of the training set as a validation set and the train/test splits are provided by the authors.

In the following, we describe how we preprocess the MegaDepth and ScanNet datasets for our experiments in Sec. 6.

**MegaDepth [39]** is a challenging large-scale outdoor dataset for depth estimation that has 3D Structure-from-Motion models for 189 landmarks. Since it consists of internet images with different camera intrinsics and image dimensions, we rescale the images to get the same focal length as the average focal length of the Cambridge Landmarks dataset. We then center-crop all rescaled images to the Cambridge image resolution, *i.e.*,  $1920 \times 1080$  pixels, where images with lower resolution than this are ignored. In total, this results in a subset of 60k images. We use images from 6 scenes for validation.

**ScanNet [17]** is a large indoor dataset containing 2.5 million views from more than 200 scenes, where we ignore scenes with less than 2500 images. Similar to 7Scenes, the views of ScanNet are densely taken. To further reduce the number of similar images, we pick one image every 5 image frames, resulting in 145k images in total. Every image is first rescaled to have the same focal length as the average of the 7Scenes dataset. The rescaled images have a resolution of  $436 \times 583$  pixels, so we add zero padding to each image to have the same resolution as the images in the 7Scenes datasets, *i.e.*,  $640 \times 480$  pixels. For ScanNet we pick half of the images from 5 scenes for validation.

### Training Pairs

To generate the training pairs required by EssNet and NC-EssNet, we use the CNN (resnet101-gem) proposed in [52] to identify  $k$  relevant images for each training/validation image from the training set.

Simply picking the top- $k$  similar images returns a set of  $k$  images which are often too similar and too close to the target image, especially for indoor scenes. Instead, we heuristically apply the following steps to obtain a more diverse

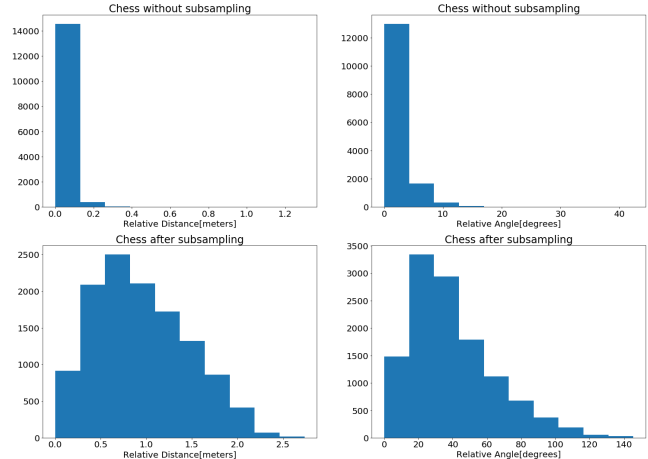


Figure 2. Comparison of relative pose distributions. We plot histograms of the difference in camera position and orientation for pairs of training images from the Chess scene. The first row shows the distribution of relative motion of pairs generated by the retrieving the top-5 similar images, resulting in only small relative translations and rotations. The second row shows the distribution after subsampling, which is much more diverse.

distribution of relative poses: 1) Select the top- $n$  similar images from the training set, where  $n$  is half of the total number of training images. 2) Split the  $n$  images equally into  $m$  subsets. 3) Subsample  $r_i * k$  images from the subset  $S_i$ , where  $i \in [0, m]$  and  $r_i$  specifies the fraction of images to pick from  $S_i$ . The parameters  $m$  and  $r_i$  are manually set for each dataset. The selection process is able to efficiently assure a diverse distribution of relative poses, which is crucial for successful supervision (see Fig. 2 as an example). To properly balance the amount of training data, we set  $k = 30$  for Cambridge and  $k = 4$  for 7Scenes. We obtain about 96k pairs for Cambridge Landmarks, and about 78k pairs for 7Scenes.

### EssNet Ablation Study

In this section, we want to validate our architectural choices and also show regressing essential matrices is a more general method than direct relative pose regression(RPR). For a fair comparison, all models are trained and tested on Cambridge Landmarks using the same training pairs. In order to train faster, we perform all trainings on a small input resolution, *i.e.*,  $224 \times 224$  and adapt the training parameters as well.

Firstly, we trained 4 EssNet models on each scene of the Cambridge Landmarks dataset, *i.e.* EssNet(PerScene). We see an obvious drop in performance compared to EssNet (trained with all scenes together). We thus train all models in our other experiments with all scenes of a dataset. We then compare EssNet with 2 EssNet variants: EssNet(Concat) replaces the matching layer [56] with concatenation operation; EssNet(NoProj) outputs essential matri-

Network	EssNet(Concat)	EssNet(NoProj)	EssNet	EssNet(PerScene)	RelaPoseNet( $\beta = 1$ )	RelaPoseNet(Learn $\beta$ )
King’sCollege	0.89/3.76	0.87/2.42	0.83/1.75	0.79/1.87	0.88/3.36	0.85/1.50
OldHospital	2.06/4.29	1.83/3.33	1.54/2.34	1.67/3.17	1.90/3.97	1.46/2.75
ShopFacade	0.84/5.26	1.08/4.37	0.74/4.39	1.21/6.79	0.98/4.25	0.85/4.16
StMary’sChurch	1.57/7.48	1.58/4.68	1.27/4.04	1.48/5.86	1.45/5.96	1.77/5.71
Average	1.34/5.20	1.34/3.70	1.10/3.13	1.29/4.42	1.30/4.39	1.23/3.53

Table 5. Ablation study of the EssNet architecture on the Cambridge Landmarks dataset.

Method	Pretrain(Task)	Finetune	Testing Datasets	
			Cambridge(CL)	7scenes(7S)
EssNet	ImageNet(IC)	CL/7S(EMR)	1.10/3.13	0.21/7.82
EssNetA	ScanNet(EMR)	7S(EMR)	-	0.22/7.68
EssNetB	MegaDepth(EMR)	CL/7S(EMR)	0.98/2.85	0.22/7.76
EssNetC	MegaDepth(EMR)	<b>CL+7S(EMR)</b>	0.98/3.03	0.21/7.64
*Learn. PN [31]	ImageNet(IC)	CL/7S(APR)	1.43/2.85	0.24/7.87
*Geo. PN [31]	CL/7S(APR)	CL/7S(APR)	1.63/2.86	0.23/8.12
Relative PN [35]	ImageNet(IC)	7S(RPR)	-	0.21/9.30
RelocNet [4]	ScanNet(IR)	7S(RPR)	-	0.21/6.73

Table 6. Leveraging external datasets on EssNet.

ces without the projection layer (*c.f.* main paper Sec.4.2). As shown in Tab. 5, EssNet clearly outperforms both EssNet(Concat) and EssNet(NoProj), which refers that matching layer is superior to a simple concatenation operation to combine feature maps for essential matrix regression, and a projection layer which brings an essential matrix approximation into a true one improves performance.

In order to fairly compare EssNet to a RPR model within our pipeline, we implement our version of the siamese network in [35] with exactly the same architecture, named as RelaPoseNet. We train it either with the original loss in [35], *i.e.*,  $\beta = 1.0$ , or the loss learning the hyperparameter during training as in [31]. As we can see in Tab. 5, setting  $\beta = 1$  does not work well for outdoor scenes, while automatically learning the weighting during the training also does not outperform EssNet. Therefore, we verify that regressing essential matrix is a superior way to fix the weighting between the translation and rotation.

### EssNet With External Datasets

It is well-known that data is essential for the success of supervised learning. For example, pretraining on the millions of annotated examples of ImageNet has become a common practice in the community. A standard **EssNet** is pretrained on ImageNet for image classification (IC) then fine-tuned on target datasets, *i.e.*, Cambridge Landmarks (CL)/7 Scenes (7S), for essential matrix regression (EMR). Similar to RelocNet [4], which shows the advantage of using more training data for training descriptors with a loss relevant to relocalisation task, we also analyze the effect of directly pretraining EssNet on an external larger dataset in Tab. 6. Note, the first column shows the method name, the second the dataset used for pretraining the network, while the third column shows the datasets used for finetuning the network.

We first pretrain EssNet on ScanNet/MegaDepth before finetuning it on 7S/CL, respectively, which leads to **EssNetA** and **EssNetB**. As from the results, while EssNetB pretrained on MegaDepth is able to improve slightly the performance on Cambridge, overall EssNet variants do not benefit much from external datasets.

Next we further investigate the training sensitivity to scene types by train a single EssNet model, *i.e.*, **EssNetC**, on a mixture of indoor and outdoor scenes, *i.e.*, **CL+7S**, which achieves state-of-the-art accuracy on **both** datasets. This again verify our method is a more general solution by eliminating the hyperparameter  $\beta$  in RPR (*c.f.* main paper Sec.4.2).

However, no matter how good EssNet performs on scenes it has been trained for, it fails to generalize to completely new unseen scenes (*c.f.* Tab.3 in main paper). This is exactly the generalization limitation of all data-driven regression-based methods we focus on in this paper.

### Implementation Details

Our approach is implemented in Pytorch 1.0 with Python 3.7 on Ubuntu 16.04.6. We will make our code publicly available.

### References

- [1] R. Arandjelović, P. Gronat, A. Torii, T. Pajdla, and J. Sivic. NetVLAD: CNN architecture for weakly supervised place recognition. In *CVPR*, 2016.
- [2] R. Arandjelović and A. Zisserman. DisLocation: Scalable descriptor distinctiveness for location recognition. In *ACCV*, 2014.
- [3] C. Arth, D. Wagner, M. Klopschitz, A. Irschara, and D. Schmalstieg. Wide area localization on mobile phones. In *ISMAR*, 2009.
- [4] V. Balntas, S. Li, and V. Prisacariu. Relocnet: Continuous metric learning relocalisation using neural nets. In *The European Conference on Computer Vision (ECCV)*, September 2018.
- [5] E. Brachmann, A. Krull, S. Nowozin, J. Shotton, F. Michel, S. Gumhold, and C. Rother. DSAC - Differentiable RANSAC for Camera Localization. In *CVPR*, 2017.
- [6] E. Brachmann, F. Michel, A. Krull, M. Y. Yang, S. Gumhold, and C. Rother. Uncertainty-driven 6d pose estimation of objects and scenes from a single rgb image. In *CVPR*, 2016.

- [7] E. Brachmann and C. Rother. Learning Less is More - 6D Camera Localization via 3D Surface Regression. In *CVPR*, 2018.
- [8] G. Bradski. The OpenCV Library. *Dr. Dobb's Journal of Software Tools*, 2000.
- [9] S. Brahmabhatt, J. Gu, K. Kim, J. Hays, and J. Kautz. Geometry-aware learning of maps for camera localization. In *IEEE Conference on Computer Vision and Pattern Recognition (CVPR)*, 2018.
- [10] F. Camposeco, A. Cohen, M. Pollefeys, and T. Sattler. Hybrid scene Compression for Visual Localization. *arXiv:1807.07512*, 2018.
- [11] S. Cao and N. Snavely. Graph-Based Discriminative Learning for Location Recognition. In *CVPR*, 2013.
- [12] S. Cao and N. Snavely. Minimal Scene Descriptions from Structure from Motion Models. In *CVPR*, 2014.
- [13] R. O. Castle, G. Klein, and D. W. Murray. Video-rate Localization in Multiple Maps for Wearable Augmented Reality. In *ISWC*, 2008.
- [14] T. Cavallari, S. Golodetz, N. A. Lord, J. Valentin, L. Di Stefano, and P. H. S. Torr. On-The-Fly Adaptation of Regression Forests for Online Camera Relocalisation. In *CVPR*, 2017.
- [15] S. Choudhary and P. J. Narayanan. Visibility probability structure from sfm datasets and applications. In *ECCV*, 2012.
- [16] R. Clark, S. Wang, A. Markham, N. Trigoni, and H. Wen. Vidloc: A deep spatio-temporal model for 6-dof video-clip relocalization. In *CVPR*, 2017.
- [17] A. Dai, A. X. Chang, M. Savva, M. Halber, T. Funkhouser, and M. Nießner. Scannet: Richly-annotated 3d reconstructions of indoor scenes. In *Proc. Computer Vision and Pattern Recognition (CVPR), IEEE*, 2017.
- [18] Z. Dang, K. Moo Yi, Y. Hu, F. Wang, P. Fua, and M. Salzmann. Eigendecomposition-free training of deep networks with zero eigenvalue-based losses. In *The European Conference on Computer Vision (ECCV)*, September 2018.
- [19] J. Deng, W. Dong, R. Socher, L.-J. Li, K. Li, and L. Fei-Fei. Imagenet: A large-scale hierarchical image database. In *Computer Vision and Pattern Recognition, 2009. CVPR 2009. IEEE Conference on*, pages 248–255. Ieee, 2009.
- [20] M. Donoser and D. Schmalstieg. Discriminative Feature-to-Point Matching in Image-Based Localization. In *CVPR*, 2014.
- [21] J. Engel, V. Koltun, and D. Cremers. Direct Sparse Odometry. *PAMI*, 2018.
- [22] M. Fischler and R. Bolles. Random sample consensus: a paradigm for model fitting with applications to image analysis and automated cartography. *CACM*, 24(6):381–395, 1981.
- [23] P. Gronat, G. Obozinski, J. Sivic, and T. Pajdla. Learning per-location classifiers for visual place recognition. In *CVPR*, 2013.
- [24] A. Guzman-Rivera, P. Kohli, B. Glocker, J. Shotton, T. Sharp, A. Fitzgibbon, and S. Izadi. Multi-Output Learning for Camera Relocalization. In *CVPR*, 2014.
- [25] R. I. Hartley and A. Zisserman. *Multiple View Geometry in Computer Vision*. Cambridge University Press, ISBN: 0521540518, second edition, 2004.
- [26] K. He, X. Zhang, S. Ren, and J. Sun. Delving deep into rectifiers: Surpassing human-level performance on imagenet classification. In *Proceedings of the IEEE international conference on computer vision*, pages 1026–1034, 2015.
- [27] K. He, X. Zhang, S. Ren, and J. Sun. Deep Residual Learning for Image Recognition. In *CVPR*, 2016.
- [28] A. Irschara, C. Zach, J.-M. Frahm, and H. Bischof. From Structure-from-Motion Point Clouds to Fast Location Recognition. In *CVPR*, 2009.
- [29] H. Jegou, M. Douze, and C. Schmid. Hamming Embedding and Weak Geometric Consistency for Large Scale Image Search. In *ECCV*, 2008.
- [30] A. Kendall and R. Cipolla. Modelling uncertainty in deep learning for camera relocalization. In *ICRA*, 2016.
- [31] A. Kendall and R. Cipolla. Geometric Loss Functions for Camera Pose Regression With Deep Learning. In *CVPR*, 2017.
- [32] A. Kendall, M. Grimes, and R. Cipolla. Posenet: A convolutional network for real-time 6-dof camera relocalization. In *ICCV*, 2015.
- [33] D. P. Kingma and J. L. Ba. Adam: A method for stochastic optimization. *ICLR*, 2015.
- [34] L. Kneip, D. Scaramuzza, and R. Siegwart. A novel parametrization of the perspective-three-point problem for a direct computation of absolute camera position and orientation. In *CVPR*, 2011.
- [35] Z. Laskar, I. Melekhov, S. Kalia, and J. Kannala. Camera Relocalization by Computing Pairwise Relative Poses Using Convolutional Neural Network. In *ICCV Workshops*, 2017.
- [36] K. Lebeda, J. Matas, and O. Chum. Fixing the Locally Optimized RANSAC. In *BMVC*, 2012.
- [37] Y. Li, N. Snavely, D. Huttenlocher, and P. Fua. Worldwide pose estimation using 3d point clouds. In *ECCV*, 2012.
- [38] Y. Li, N. Snavely, and D. P. Huttenlocher. Location Recognition Using Prioritized Feature Matching. In *ECCV*, 2010.
- [39] Z. Li and N. Snavely. Megadepth: Learning single-view depth prediction from internet photos. In *Computer Vision and Pattern Recognition (CVPR)*, 2018.
- [40] H. Lim, S. N. Sinha, M. F. Cohen, and M. Uyttendaele. Real-time image-based 6-dof localization in large-scale environments. In *CVPR*, 2012.
- [41] D. Lowe. Distinctive image features from scale-invariant keypoints. *IJCV*, 60(2):91–110, 2004.
- [42] S. Lynen, T. Sattler, M. Bosse, J. Hesch, M. Pollefeys, and R. Siegwart. Get Out of My Lab: Large-scale, Real-Time Visual-Inertial Localization. In *RSS*, 2015.
- [43] I. Melekhov, J. Ylioinas, J. Kannala, and E. Rahtu. Image-based Localization using Hourglass Networks. In *ICCV Workshops*, 2017.
- [44] I. Melekhov, J. Ylioinas, J. Kannala, and E. Rahtu. Relative camera pose estimation using convolutional neural networks. In *International Conference on Advanced Concepts for Intelligent Vision Systems*, pages 675–687, 2017.
- [45] L. Meng, J. Chen, F. Tung, J. J. Little, J. Valentin, and C. W. de Silva. Backtracking Regression Forests for Accurate Camera Relocalization. In *IROS*, 2017.

- [46] K. Moo Yi, E. Trulls, Y. Ono, V. Lepetit, M. Salzmann, and P. Fua. Learning to Find Good Correspondences. In *CVPR*, 2018.
- [47] R. Mur-Artal, J. M. M. Montiel, and J. D. Tardos. ORB-SLAM: A Versatile and Accurate Monocular SLAM System. *TRO*, 31(5):1147–1163, 2015.
- [48] T. Naseer and W. Burgard. Deep regression for monocular camera-based 6-dof global localization in outdoor environments. In *IROS*, 2017.
- [49] D. Nister. An efficient solution to the five-point relative pose problem. In *2003 IEEE Computer Society Conference on Computer Vision and Pattern Recognition, 2003. Proceedings.*, volume 2, pages II–195. IEEE, 2003.
- [50] A. Paszke, S. Gross, S. Chintala, G. Chanan, E. Yang, Z. DeVito, Z. Lin, A. Desmaison, L. Antiga, and A. Lerer. Automatic differentiation in pytorch. In *NIPS-W*, 2017.
- [51] J. Philbin, O. Chum, M. Isard, J. Sivic, and A. Zisserman. Object retrieval with large vocabularies and fast spatial matching. In *CVPR*, 2007.
- [52] F. Radenović, G. Toliás, and O. Chum. CNN image retrieval learns from BoW: Unsupervised fine-tuning with hard examples. In *ECCV*, pages 3–20, 2016.
- [53] F. Radenović, G. Toliás, and O. Chum. Fine-tuning CNN image retrieval with no human annotation. *TPAMI*, 2018.
- [54] R. Ranftl and V. Koltun. Deep fundamental matrix estimation. In *Proceedings of the European Conference on Computer Vision (ECCV)*, pages 284–299, 2018.
- [55] I. Rocco, R. Arandjelović, and J. Sivic. Convolutional neural network architecture for geometric matching. In *Proceedings of the IEEE Conference on Computer Vision and Pattern Recognition*, 2017.
- [56] I. Rocco, M. Cimpoi, R. Arandjelović, A. Torii, T. Pajdla, and J. Sivic. Neighbourhood consensus networks. In *Proceedings of the 32nd Conference on Neural Information Processing Systems*, 2018.
- [57] O. Russakovsky, J. Deng, H. Su, J. Krause, S. Satheesh, S. Ma, Z. Huang, A. Karpathy, A. Khosla, M. Bernstein, A. C. Berg, and L. Fei-Fei. ImageNet Large Scale Visual Recognition Challenge. *IJCV*, 115(3):211–252, 2015.
- [58] S. Saha, G. Varma, and C. V. Jawahar. Improved Visual Relocalization by Discovering Anchor Points. In *BMVC*, 2018.
- [59] T. Sattler, M. Havlena, F. Radenović, K. Schindler, and M. Pollefeys. Hyperpoints and Fine Vocabularies for Large-Scale Location Recognition. In *ICCV*, 2015.
- [60] T. Sattler, B. Leibe, and L. Kobbelt. Efficient & Effective Prioritized Matching for Large-Scale Image-Based Localization. *PAMI*, 39(9):1744–1756, 2017.
- [61] T. Sattler, W. Maddern, C. Toft, A. Torii, L. Hammarstrand, E. Stenborg, D. Safari, M. Okutomi, M. Pollefeys, J. Sivic, F. Kahl, and T. Pajdla. Benchmarking 6DOF Outdoor Visual Localization in Changing Conditions. In *CVPR*, 2018.
- [62] T. Sattler, A. Torii, J. Sivic, M. Pollefeys, H. Taira, M. Okutomi, and T. Pajdla. Are Large-Scale 3D Models Really Necessary for Accurate Visual Localization? In *CVPR*, 2017.
- [63] T. Sattler, Q. Zhou, M. Pollefeys, and L. Leal-Taixe. Understanding the Limitations of CNN-based Absolute Camera Pose Regression. *arxiv:1903.07504*, 2019.
- [64] J. L. Schönberger and J.-M. Frahm. Structure-from-motion revisited. In *CVPR*, 2016.
- [65] J. L. Schönberger, M. Pollefeys, A. Geiger, and T. Sattler. Semantic Visual Localization. In *CVPR*, 2018.
- [66] J. L. Schönberger, M. Pollefeys, A. Geiger, and T. Sattler. Semantic Visual Localization. In *CVPR*, 2018.
- [67] J. Shotton, B. Glocker, C. Zach, S. Izadi, A. Criminisi, and A. Fitzgibbon. Scene coordinate regression forests for camera relocalization in rgb-d images. *CVPR*, 2013.
- [68] J. Sivic and A. Zisserman. Video Google: A text retrieval approach to object matching in videos. In *ICCV*, 2003.
- [69] L. Svärm, O. Enqvist, F. Kahl, and M. Oskarsson. City-Scale Localization for Cameras with Known Vertical Direction. *PAMI*, 39(7):1455–1461, 2017.
- [70] H. Taira, M. Okutomi, T. Sattler, M. Cimpoi, M. Pollefeys, J. Sivic, T. Pajdla, and A. Torii. InLoc: Indoor Visual Localization with Dense Matching and View Synthesis. In *CVPR*, 2018.
- [71] C. Toft, E. Stenborg, L. Hammarstrand, L. Brynte, M. Pollefeys, T. Sattler, and F. Kahl. Semantic Match Consistency for Long-Term Visual Localization. In *ECCV*, 2018.
- [72] A. Torii, R. Arandjelović, J. Sivic, M. Okutomi, and T. Pajdla. 24/7 place recognition by view synthesis. In *CVPR*, 2015.
- [73] A. Torii, J. Sivic, and T. Pajdla. Visual localization by linear combination of image descriptors. In *ICCVW*, 2011.
- [74] A. Torii, J. Sivic, T. Pajdla, and M. Okutomi. Visual place recognition with repetitive structures. In *CVPR*, 2013.
- [75] B. Ummenhofer, H. Zhou, J. Uhrig, N. Mayer, E. Ilg, A. Dosovitskiy, and T. Brox. DeMoN: Depth and Motion Network for Learning Monocular Stereo. In *CVPR*, 2017.
- [76] J. Valentin, M. Nießner, J. Shotton, A. Fitzgibbon, S. Izadi, and P. Torr. Exploiting Uncertainty in Regression Forests for Accurate Camera Relocalization. In *CVPR*, 2015.
- [77] F. Walch, C. Hazirbas, L. Leal-Taixe, T. Sattler, S. Hilsenbeck, and D. Cremers. Image-based localization using lstms for structured feature correlation. In *ICCV*, 2017.
- [78] T. Weyand, I. Kostrikov, and J. Philbin. Planet - photo geolocation with convolutional neural networks. *ECCV*, 2016.
- [79] C. Wu. Towards linear-time incremental structure from motion. In *3DV*, 2013.
- [80] A. R. Zamir and M. Shah. Accurate image localization based on google maps street view. In *ECCV*, 2010.
- [81] A. R. Zamir and M. Shah. Image Geo-Localization Based on Multiple Nearest Neighbor Feature Matching Using Generalized Graphs. *PAMI*, 36(8):1546–1558, 2014.
- [82] B. Zeisl, T. Sattler, and M. Pollefeys. Camera pose voting for large-scale image-based localization. In *ICCV*, 2015.
- [83] W. Zhang and J. Kosecka. Image based localization in urban environments. In *3DPVT*, 2006.
- [84] T. Zhou, M. Brown, N. Snavely, and D. G. Lowe. Unsupervised Learning of Depth and Ego-Motion From Video. In *CVPR*, 2017.